Activation transport under quantum Hall regime in HgTe-based heterostructure

S.V. Gudina[1], V.N. Neverov[1], E.G. Novik[2], E.V. Ilchenko[1], G.I. Harus[1], N.G. Shelushinina[1], S.M. Podgornykh[1,3], M.V. Yakunin[1,3], N.N. Mikhailov[4,5], and S.A. Dvoretsky[4,6]

[1]*M.N. Mikheev Institute of Metal Physics, Ural Branch, Russian Academy of Sciences*
18 S. Kovalevskaya Str., Ekaterinburg 620137, Russia
E-mail: ilchenko@imp.uran.ru

[2]*Physikalisches Institut (EP3), University of Würzburg, Würzburg 97074, Germany*

[3]*B.N. Yeltsin Ural Federal University, 19 Mira Str., Ekaterinburg 620002, Russia*

[4]*A.V. Rzhanov Institute of Semiconductor Physics, Siberian Branch, Russian Academy of Sciences*
13 Akad. Lavrent'eva Ave., Novosibirsk 630090, Russia

[5]*Novosibirsk State University, 2 Pirogova Str., Novosibirsk 630090 Russia*

[6]*National Research Tomsk State University, 36 Lenina Ave., Tomsk 634050, Russia*

We have measured the temperature ($2.9\ \text{K} < T < 50\ \text{K}$) and magnetic field ($0\ \text{T} < B < 9\ \text{T}$) dependences of longitudinal and Hall resistivities for HgCdTe/HgTe/HgCdTe system with HgTe quantum well width of 20.3 nm. The activation analysis of the experimental magnetoresistivity traces has been used as a quantitative tool to probe inter-Landau level distances. The activation energies were determined from the temperature dependence of the longitudinal resistivity in the regions of quantized Hall plateaus (for the filling factors ν of 1, 2 and 3) and the indications of the large values of the g factor $\cong$ 30–75 were found.

1. Introduction

Heterostructures of HgTe and CdTe are of type III combining a positive band gap semiconductor (CdTe) and a zero-gap semimetal (HgTe) with gaps formed between states of Γ8 and Γ6 symmetry. In recent years, high-mobility HgTe-based heterostructures have become available for experimental investigations due to advances in the molecular beam epitaxy (MBE) technology (see, for example, [1] and references therein). Layered quantum structures of HgTe and CdTe attracted interest due to the rich possibilities for band structure species.

Depending on their thicknesses, single HgTe quantum well (QW) between CdTe (or HgCdTe with a large energy gap) barriers can exist in two distinct regimes [1]. For small QW widths and thus larger subband separations, an open gap is formed between heavy-hole subband (*H*1) and an electron-like light-particle subband (*E*1) that corresponds to the normal regime. With increasing QW width the *E*1 subband falls below the topmost heavy-hole subbands and takes on hole-like character, while the *H*1 subband becomes electron-like. Such QWs are in the inverted-band regime. The inverted regime is achieved when QW width, d_{QW}, exceeds a critical value $d_c \cong 6.3$ nm.

In the latter case the conduction band exhibits Γ8 symmetry with a coupling heavy-hole to light-particle states at finite inplane wave vectors. That leads to a complex Landau level (LL) spectra as a quantizing magnetic field uncovers the mixed nature of the *H*1 subband in the inverted-band regime [2].

It is known that the effective probing of the LL fan diagram can be realized by means of the activation mag-

netotransport analysis under the quantum Hall (QH) regime. Distances between adjacent LLs can be extracted and a density of localized states in the mobility gaps may be determined from scanning them by the Fermi level in experiments of this kind [3–7]. Experimental reconstruction of the energy spectrum is especially important for systems with a complex band structure where the LL picture is determined not only by the cyclotron energy with a given effective mass as for a simple parabolic conduction band system.

As for the HgTe-based 2D structures, in [8] the activation energies were determined from the temperature dependence of the longitudinal resistivity in the regions of quantized Hall plateaus (for the filling factors ν of 1 and 2) in a 6.6 nm HgTe quantum well at magnetic fields up to 34 T at nitrogen temperatures. The indications of the large values of the *g* factor (about 30–40) were found.

In [9] the quantum Hall effect (QHE) in HgTe QWs with a finite band gap below and above the critical thickness d_c (d_{QW} = 5.9 nm and 11 nm) has been studied up to temperatures of the order of 50 K. From temperature dependent magnetotransport measurements, they extracted the energy gaps between LLs of the order of 40–45 meV for ν = 1 and of the order of 25 meV for ν = 2, in good agreement with the Landau level spectrum obtained from **k·p** calculations.

In our previous paper [10] we have studied the QHE plateau–plateau transition for a wide temperature range T = 2.9–50 K at HgCdTe/HgTe/HgCdTe system with the inverted band structure. In subsequent work [11] the first study of variable-range hopping conductivity at the QHE plateau regions in the HgTe/HgCdTe heterostructure has been done. The present work is devoted to a probing of HqTe quantum well LL spectrum at the same system by means of the quantum Hall effect.

2. Characteristics of the sample

We present a study of quantum magnetotransport in a 20.3-nm-wide HgTe QW grown on the (013) GaAs substrate, symmetrically modulation doped with In at both sides at distances of about 10-nm spacers. The electron gas density is n_S = 1.5·10^{11} cm^{-2} with a mobility of 22 m^2/(V·s).

The 2DEG in wide HgTe quantum well ($d > d_c \cong$ $\cong$ 6.3 nm) is characterized by a highly specific energy spectrum with an inverted band structure, low effective mass $m_{eff} \approx$ (0.02–0.03)m_0 (m_0 being free electron mass) and, consequently, a large Landau level separation. In [12] a review of the bulk HgTe and CdTe bandstructure and a simple model for the physics of the relevant subbands of HgTe/CdTe QW are presented.

In the inverted regime of HgTe QW the first size-quantized heavy-hole subband *H*1 becomes the lowest conduction band as the theory [13,14] predicts an electron-like effective mass for it. The highest valence band is now

the second size-quantized heavy-hole subband *H*2 with nonmonotonic dispersion law [13,14].

A substantial overlap about 6.45 meV of the valence *H*2 and conduction *H*1 subbands is obtained when the strain is considered in calculations, but this overlap would not be felt experimentally in a single QW at electron densities $n \gtrsim 1.5 \cdot 10^{11}$ cm^{-2} since the Fermi level is above the overlap region.

In the system we studied the conduction is carried out just by the electrons of band *H*1 with extremely small value of the effective mass of carriers: for n_S = 1.5·10^{11} cm^{-2} mass at the Fermi level m_{eff} = (0.022–0.026)m_0 [15,16] and with a large value of *g* factor, $g \cong$ 50 [16].

The Landau level spectra for investigated structure HgTe/Hg$_{0.35}$Cd$_{0.65}$Te ([001]) QW calculated within the axial approximation is shown on Fig. 1. The LL notations correspond to the notations of [2].

It is seen that the Landau levels are of the essence no equidistant and nonlinear on magnetic field which caused by the mixed nature of the *H*1 and *H*2 subbands in the inverted-band regime due to a coupling between heavy-hole to light-particle states at finite inplane wave vectors $k_\parallel$. Only the lowest Landau level ($N = -2\downarrow$) of the *H*1 subband contains pure heavy-hole states which do not mix with the light-particle states [9] (see also [17] and references therein).

In [17] it is shown that this level is of the same nature in two and in three dimensions and it is mapped on the *b* set level of Guldner *et al.* [18] $E_b(0) = (e\hbar B/m)\varepsilon_b(0)$, where

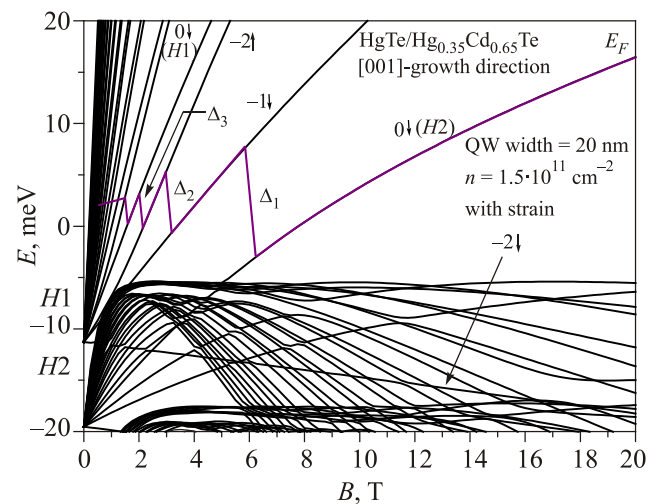$$\varepsilon_b(0) = \frac{1}{2}(\gamma_1 + \overline{\gamma}) - \frac{3}{2}\kappa. \qquad (1)$$

Fig. 1. (Color online) Landau levels of *H*1 and *H*2 subbands for an *n*-type HgTe/Hg$_{0.3}$Cd$_{0.7}$Te (001) QW as a function of magnetic field within the axial approximation; d_W = 20 nm, n_{2DEG} = = 1.5·10^{11} cm^{-2}. The Landau levels are labeled in accordance with the notations of [2]: the quantum numbers $N = -2, -1, 0, \ldots$, and the arrows (↑, ↓) indicate the dominant spin orientation of the state. The thick line represents the chemical potential.

For the set of Γ_8 Luttinger parameters for HgTe ($\gamma_1 = 12.8$, $\overline{\gamma} = 8.4$ and $\kappa = 10.5$ [18]) we have

$$3\kappa > \left(\gamma_1 + \overline{\gamma}\right), \qquad (2)$$

and, according to (1), the level $N = -2\!\downarrow$ lowers its energy linearly with increasing magnetic field revealing a hole-like character. All the other Landau levels of the $H1$ subband show an electron-like character: they rise in energy with magnetic field due to the coupling with light-particle states.

Figure 1 shows also that the Landau level of the $H2$ subband with $N = 0\!\downarrow$ becomes the highest $H2$ LL at $B \gtrsim 5$ T in consequence of a distinct mixing of the heavy and the light states [19]. The unusual behavior of $N = -2\!\downarrow$ level from the conduction subband $H1$ in inverted band HgTe QWs together with the peculiar dispersion of the $N = 0\!\downarrow$ level from the topmost valence subband $H2$ leads to a crossing of conduction- and valence-subband states at a some value B_c of the magnetic field (see Fig. 1).

Such behavior is specific for HgTe QWs and has been examined theoretically and experimentally (see, for example, [20]). In our structure the lowest $N = -2\!\downarrow$ LL of the $H1$ conduction subband and the $N = 0\!\downarrow$ LL of the $H2$ valence subband cross at $B_c \approx 2.5$ T, and the point of intersection is immersed in the thick of valence band Landau levels (see Fig. 1). As a consequence, the $N = -2\!\downarrow$ level is irrelevant in our situation and in the actual region of our study at $B \gg B_c$ just the $N = 0\!\downarrow$ level of the $H2$ subband appears as the lowest Landau level of the conduction band.

Thus, a peculiarity of HgTe QWs in the inverted-band regime is that nominally (in labeling of the Landau level by the dominant spin component at energies near the $H1$ bottom) the spin splitting in the $H1$ conduction subband turns out to be larger than the orbital splitting which is particularly evident from a scheme on the inset of Fig. 4. Such a relation of spin and cyclotron splittings is a consequence of specific numerical values for Luttinger parameters in HgTe (see Eqs. (1), (2)).

Note, that for Ge the values of Γ_8 Luttinger parameters ($\gamma_1 = 13.38$, $\overline{\gamma} = 4.96$ and $\kappa = 3.41$ [21]) are such that

$$3\kappa < \left(\gamma_1 + \overline{\gamma}\right), \qquad (3)$$

and thus for the QW based on p-Ge the highest valence Landau level $E_b(0) = -(e\hbar B/m)\varepsilon_b(0)$ have the same energy dispersion as all other hole LL of a spatially quantized valence band [17].

Our further plan is as follows: first, to determine the activation energies of longitudinal resistivity ρ_{xx} in the QHE regime for $\nu = 1$ (the gap between $N = 0\!\downarrow$ LL of $H2$ subband and $N = -1\!\downarrow$ LL of the $H1$ subband), $\nu = 2$ (gap $N = -1\!\downarrow \rightarrow N = -2\!\uparrow$ of the $H1$ subband) and $\nu = 3$ (gap $N = -2\!\uparrow \rightarrow N = 0\!\downarrow$ of the $H1$ subband) and then, to estimate the background density of states (DOS) in these mobility gaps.
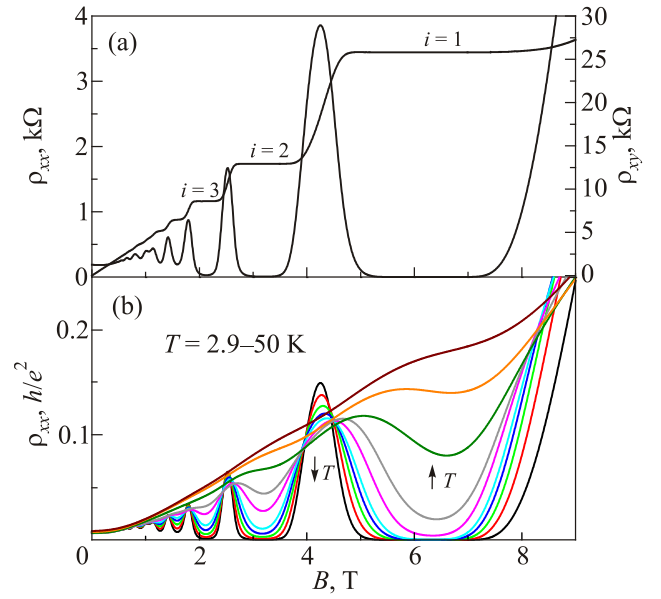

Fig. 2. (Color online) The longitudinal and Hall resistivity dependencies on the magnetic field B at 2.9 K (i signifies a number of the QHE plateau) (a). The longitudinal resistivity at $T = 2.9$–50 K (b).

3. Experimental results and discussions

We used the method of thermally activated magnetoresistivity for reconstruction of the 2D electron gas (2DEG) spectrum under quantizing magnetic fields at a wide HgTe QW with the inverted band structure at HgCdTe/HgTe/HgCdTe system. Measurements of the longitudinal ρ_{xx} and Hall ρ_{xy} resistivities have been carried out in magnetic fields up to 9 T at $T = 2.9$–50 K (Fig. 2).

Figure 2(a) gives the magnetic-field dependences of the ρ_{xx} and ρ_{xy} resistivities for the sample under study at $T = 2.9$ K. We can see the features characteristic of the QHE regime, i.e., the regions of plateau in the $\rho_{xy}(B)$ dependences with corresponding deep minimum of $\rho_{xx}(B)$ for filling factors up to $\nu = 3$.

Figure 2(b) shows the magnetic-field dependences of the longitudinal ρ_{xx} resistivity for investigated sample at $T = 2.9$–50 K. The thermally activated conduction may be seen in the magnetic field range of the Hall plateaux.

3.1. Activation energies

The appearance of quantized plateaux in the $\rho_{xy}(B)$ dependences with vanishing values of ρ_{xx} is now commonly accepted to be caused by the existence of disorder-induced mobility gaps in the DOS of a 2D system in high magnetic field.

When the Fermi level in the QHE regime is settled down in the gap between adjacent LLs, the thermally activated behavior of ρ_{xx} (or σ_{xx}) is observed due to the excitation of electrons to the narrow band of extended states (with a width Γ) near the middle of a disorder-broadened LL.

As a rule, an assumption is used that the delocalized states with discrete energies $E = E_N$ are separated by the (mobility) gap $\Delta \gg k_B T$, that leads to an expression [3–5]:

$$\sigma_{xx}(T) \sim \exp\frac{-E_A}{k_B T} \qquad (4)$$

with $E_A = |E_F - E_N|$.

Activation behavior of the conductivity $\sigma_{xx}(T)$ for investigated sample in vicinity of $\nu = 1$ and 2 is illustrated by Figs. 3(a), (b). Figures show a fit of $\sigma_{xx}(T)$ dependencies by the Arrhenius equation (4) (straight lines in figure) in the range of more than one (for $\nu = 2$) or even three (for $\nu = 1$) orders of conductivity at $T > 10$ K. Deviations of experimental points from straight lines for $T \leq 10$ K are explained by variable range hopping among localized states at E_F, which usually dominates for sufficiently low T (see Ref. 11).

The activation energy E_A as a function of B for the filling factor ν in the vicinity of $\nu = 1$, $\nu = 2$ and $\nu = 3$ for investigated sample is presented in Fig. 4. The activation energy achieves its maximum value $E_a^{\max}$ at integer value of ν. The mobility gap width estimated as $\Delta = 2E_a^{\max}$ is closely related to the energy separation between the adjacent LLs: $\Delta = |E_N - E_{N'}|$ within the uncertainty of the order of Γ. A scheme of the orbital and spin splitting for the $H1$ conduction subband is given at the inset.

Figure 4 shows a comparison of the extracted activation energies with theoretical calculations of the LL dispersions from the Fig. 1 the calculated values of halfgaps, $\Delta_\nu/2$, for $\nu = 1$, 2 and 3 are marked by asterisks on the figure (see also Table 1). It is seen that the experimentally and theoretically obtained energy gaps are in reasonably good agreement and thus the behavior of the sample is well described
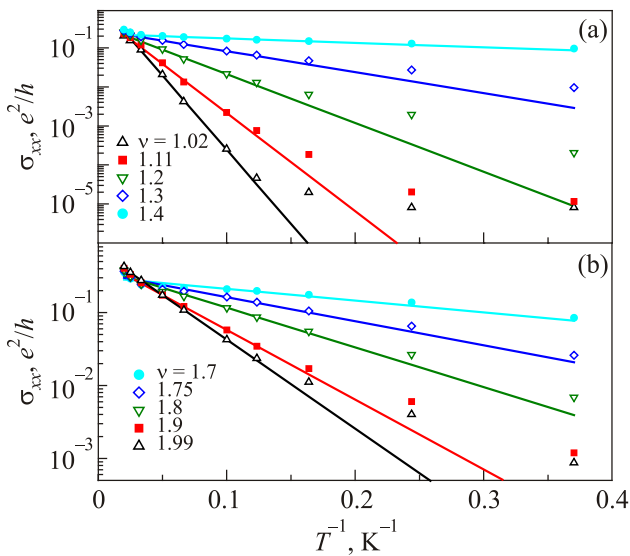

Fig. 4. The magnetic field dependence of experimentally extracted activation energies and theoretically calculated halves of energy gap values for $\nu = 1$, 2 and 3 (asterisks). Inset: a scheme of spin level layout for heavy-hole subbands $H1$ and $H2$ at investigated structure.

by our **k·p** model. In particular, We don't observe an explicit manifestation of a strong Rashba spin-orbit splitting caused by an asymmetry of QW confinement potential (see Fig. 1 in [2]).

3.2. Estimation of parameters

Let us analyze the obtained results in more details. For $\nu = 1$ we have a gap between $N = 0\downarrow$ LL of $H2$ subband and $N = -1\downarrow$ LL of the $H1$ subband at $B_1 = 6.3$ T and it is seen geometrically from Fig. 1 that Δ_1 should be close in magnitude to the gap between the heavy-hole size-quantized levels $H1$ and $H2$ at $B = 0$:

$$\Delta_1 \cong E_{H1} - E_{H2} = 3\varepsilon_h, \qquad (5)$$

where $\varepsilon_h = \dfrac{\pi^2}{2}\dfrac{h^2}{m_{hh}d^2}$, m_{hh} being the bulk heavy-hole mass. For $m_{hh} = 0.25\,m_0$ [18] and $d = 20$ nm we have $3\varepsilon_h = 9.6$ meV that is really close to the experimental value of $\Delta_1 \approx 12$ meV.

Fig. 3. (Color online) Plot of σ_{xx} versus $1/T$ in semi logarithmic scale at the high (a) and the low (b) field side of $1 \rightarrow 2$ transition. Solid lines are fit of the data by a law of Eq. (4).
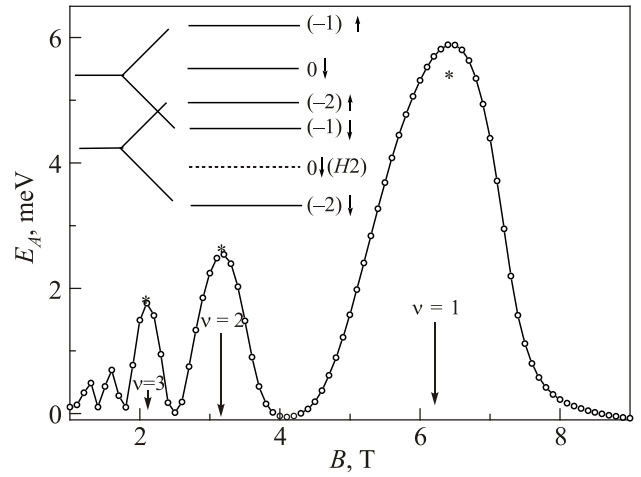
Table 1. The values of magnetic fields, B_ν, of the experimentally obtained activation energies, E_A, and corresponding gaps, $\Delta_\nu^{\exp} = 2E_A$, of calculated energy gaps, Δ_ν^{teor}, and background DOS, D_ν, at LL filling factor $\nu = 1$, 2 and 3

Parameters	$\nu = 1$	$\nu = 2$	$\nu = 3$
B_ν, T	6.3	3.15	2.1
E_A, meV	6	2.4	1.5
Δ_ν^{teor}, meV	11.6	6.9	3.8
$\Delta_\nu^{\exp}$, meV	12	4.8	3
D_ν, 10^{10}cm$^{-2}\cdot$meV^{-1}	0.64 ± 0.1	0.64 ± 0.05	0.64 ± 0.05

Note that the value of the energy gap at $\nu = 1$, $\Delta_1 \approx 40$ meV, extracted in [9] for HgTe QW with $d = 11$ nm, corresponds well to the estimation by formula (5).

Now we consider the behavior of the mobility gaps between LLs corresponding to filling factors $\nu = 2$ and $\nu = 3$. In accordance with a scheme of LL levels (see inset on Fig. 4) we have:

$$\Delta_2 = \Delta_Z(B_2) - \Delta_c(B_2) \tag{6a}$$

and

$$\Delta_3 = 2\Delta_c(B_3) - \Delta_Z(B_3). \tag{6b}$$

Here Δ_c and Δ_Z are cyclotron and Zeeman splitting, respectively, with $\Delta_c = \hbar\omega_c$, $\omega_c = eB/m_c$, m_c being electron effective mass on the Fermi level, and $\Delta_Z = g\mu_B B$, g is Lande factor, $\mu_B = e\hbar/2m_0$ is Bohr magneton; $B_2 = 3.15$ T and $B_3 = 2.1$ T. Using the experimental values of Δ_2 and Δ_3 (see Table 1) and neglecting the B-dependence of effective mass and g factor for $B_3 < B < B_2$, we get the following estimates for the parameters: $m_c/m_0 = 0.037 \pm 0.005$ and $g = 75 \pm 5$.

Note, in a case that Zeeman splitting is under the cyclotron one in the $H1$ subband (see a scheme of LL levels on the Fig. 1 in Ref. 16) we would have

$$\Delta_2 = \Delta_c(B_2) - \Delta_Z(B_2) \tag{7a}$$

and

$$\Delta_3 = \Delta_Z(B_3). \tag{7b}$$

Then the following values of the parameters would be received: $m_c/m_0 = 0.037$ (the same as in a former case) and $g = 28 \pm 2$.

It is known that the theoretical values of parameters at the bottom of a heavy-hole 2D-subband are [22–25]: $g = 6\kappa$ ($\cong 60$ for HgTe) and $m_0/m_c = (\gamma_1 + \overline{\gamma})$ ($m_c/m_0 = 0.047$ for HgTe). But the estimations of the cyclotron and Zeeman energy from the activation analysis in high magnetic fields may strongly contradict these values of g and m_c/m_0 as well as the estimations of the cyclotron energy from the weak field Shubnikov–de Haas (SdH) oscillations due to a mixed nature of heavy-hole subbands at finite $k_\parallel$ that leads to a pronounced nonlinearity of the B dependence of the LLs in the inverted-band regime.

The experimentally obtained g and m_c/m_0 values for the inverted-band HgTe QWs are somewhat contradictory and depend on the density of 2D electrons and the width of QW.

Thus, for relatively narrow QWs it was found that $g = |20|\pm5$ for symmetrically doped samples with $d = 9$ nm ($n = 6.6\cdot10^{11}$ cm^{-2}) [26] and $g \approx 20$ for 11-nm-thick HgTe QW ($n = 4.66\cdot10^{11}$ cm^{-2}) [9]. For a wide HgTe QW with $d = 20$ nm ($n = 1.5\cdot10^{11}$ cm^{-2}) a value of $|g| = 50$–60 is obtained [16].

In [26] the cyclotron mass was determined from the temperature dependence of the SdH oscillations at low magnetic fields in six n-type modulation doped HgTe single quantum wells ($d = 4.5$ nm). The obtained effective masses are: $0.025m_0$ at $n = (4-6)\cdot10^{11}$ cm^{-2} and $0.034m_0$ at $n = 1\cdot10^{12}$ cm^{-2} in accordance with the theoretical calculations of the semi-classical cyclotron mass based on a 8×8 **k·p** model.

In [27] the effective mass m has been deduced from the temperature dependence of the amplitudes of the Shubnikov–de Haas (SdH) oscillations to be $m = 0.026$ and $0.030m_0$ for 11 nm-QW ($n = 3.45\cdot10^{11}$ cm^{-2}) and 9 nm-QW ($n = 6.6\cdot10^{11}$ cm^{-2}), respectively, in good agreement with the values of $m = 0.0265$ and 0.0303 m_0, calculated by the authors in the framework of the 8×8 **k·p** model.

Far-infrared cyclotron resonance photoconductivity (CRP) have been investigated in [28] for HgTe quantum wells of three different widths: 8, 16 and 21 nm. Compared to determination of effective masses by the temperature dependence of SdH oscillations used so far in this material the authors demonstrate that CRP provides a more accurate (about few percents) tool. They found cyclotron resonance effective mass as a function of the density of 2D electrons: in each sample it increases from the value $(0.0260 \pm 0.0005)m_0$ at $n = 2.2\cdot10^{11}$ cm^{-2} to $(0.0335 \pm 0.0005)m_0$ at $n = 9.6\cdot10^{11}$ cm^{-2}.

3.3. Density of states in mobility gaps

In addition to the description of Landau level picture, a direct determination of the density of localized states (DOS) in the mobility gaps is possible from the activation analysis.

The DOS in mobility gaps may be evaluated from the data on activation energy E_A as a function of the LL filling factor ν [3–6]. As $\nu = n/n_B$ (n is the electron density, $n_B = eB/hc$ is the degree of LL degeneracy), the filling factor can be tuned by the change of either a carrier density [3] or a magnetic field [4–6].

From the $E_A(B)$ dependences the background density of states in the mobility gap may be constructed [4,6,29]:

$$D_\nu(E_F) = \left[\frac{dE_A}{dn}\right]^{-1} = \frac{\nu e}{2\pi\hbar c}\left(\frac{dE_A(B)}{dB}\right)^{-1}.$$

Figure 5 shows the results for the DOS at mobility gaps Δ_1, Δ_2, and Δ_3 (see also Table 1). The following features of the mobility gap DOS as a function of energy, $D(E)$, should be mentioned. Even in the middle of a gap when the filling factor is close to an integer, the density of localized states is found to have an unexpectedly high values comparable with the DOS of 2DEG without magnetic field (for a single spin direction):

$$D_0 = m/2\pi\hbar^2 = \frac{m}{m_0}1.3\cdot10^{26}\ \text{erg}^{-1}\cdot\text{cm}^{-2} =$$
$$= \frac{m}{m_0}2.1\cdot10^{12}\ \text{meV}^{-1}\cdot\text{cm}^{-2},$$

which gives $D_0 = 0.63\cdot10^{10}$ meV$^{-1}\cdot$cm^{-2} for $m = 0.03m_0$.

Moreover, $D(E)$ remains almost constant in the overwhelming part of the energy intervals between adjacent LL: $D(E) = (0.58–0.64)\cdot10^{10}$ cm$^{-2}\cdot$meV$^{-1} \cong D_0$ for $n = 1, 2$ and 3 (Fig. 5).

The main result that $D(E)$ is practically constant and comparable with D_0 within the energy interval between adjacent LL's is consistent with the data for structures with *n*-type conductivity: Si-MOSFET [3], high-mobility [4] and intermediate-mobility [29] AlGaAs/GaAs, InGaAs/InP [5] as well as for multilayer *p*-Ge/Ge$_{1-x}$Si$_x$ heterostructures [6].

As all short-range impurity potential models lead to an exponential drop in DOS between Landau levels, the clear picture for the DOS in QHE regime may be presented only in terms of the long-range potential fluctuations in combination with the oscillating dependence of DOS on the filling factor. Such idea has been advanced in early work of Shklovskii and Efros [30] and then developed in series of works of Efros with collaborators (see [31,32] and references therein).

In selectively doped heterostructures, the smooth random potential is formed by fluctuations in concentration of remote impurities. When the filling factor is close to an integer very small concentration of electrons, $n << n_B$, can be redistributed in space and thus one occurs in conditions of so called nonlinear screening [30–32] ("threshold" screening in terms of [33]).

For integer ν exactly the screening is realized only due to electrons (and holes) induced by an overlap of adjacent fluctuating Landau levels, and so the amplitude of random potential is of the order of corresponding LL gap. Consequently the apparent (averaged over the sample) background DOS becomes of the order of D_0.

It is considered that for the filling factors close to half integers (the regions of plateau to plateau transition) the potential fluctuations would be small due to effective (linear) electron screening [30–33].
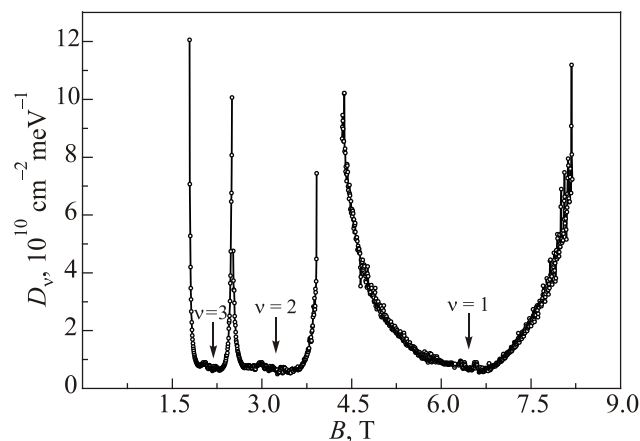

Fig. 5. The background density of states D_ν for the investigated sample, as deduced from the activation energy dependence on B, the integer ν = 1, 2 and 3 corresponds to the middle of an energy interval between two LLs.

4. Conclusions

Reach information concerning QWs in the 2D heterosystem may be obtained from the study of magnetotransport in the quantum Hall regime. In comparison with a usual analysis of the experimental magnetoresistivity traces the activation analysis yields an accurate quantitative tool to probe inter-LL distances and to estimate the background density of states in mobility gap between adjacent LLs.

We have investigated the activated magnetotransport in the QHE plateau regions at the HgCdTe/HgTe/HgCdTe system with the inverted band structure in magnetic fields up to 9 T for a wide temperature range $T = 2.9$–50 K, which turned out possible owing to the high-energy scale of the quantum Hall effect in HgTe.

The activation energies of ρ_{xx} in the QHE regime for the gap between $N = 0\downarrow$ LL of heavy-hole subband $H2$ and $N = -1\downarrow$ LL of heavy-hole subband $H1$ (ν = 1) and for the gaps $N = -1\downarrow \rightarrow N = -2\uparrow$ (ν = 2) and $N = -2\uparrow \rightarrow N = 0\downarrow$ (ν = 3) of the $H1$ subband were determined. It is shown that the experimentally obtained energy gaps are well described within the framework of **k·p** model.

Activated behavior in the quantum Hall regime also yields the background DOS that characterizes random potential distribution in the system.

Note that the temperature ranges where the QHE is still observed are significantly different for various materials: from liquid- and subliquid-helium temperatures for III–V structures to room temperatures for single-layer graphene (see, e.g., [34]). For the studied structure based on HgTe, the QHE range extends up to nitrogen temperatures (see, e.g., [8]) due to large cyclotron and Zeeman splittings.

1. M. Konig, S. Wiedmann, C. Brne, A. Roth, H. Buhmann, L.W. Molenkamp, X.-L. Qi, and S.-C. Zhang, *Science* **318**, 766 (2007).

2. E.G. Novik, A. Pfeuffer-Jeschke, T. Jungwirth, V. Latussek, C.R. Becker, G. Landwehr, H. Buhmann, and L.W. Molenkamp, *Phys. Rev. B* **72**, 035321 (2005).

3. M.G. Gavrilov and T.V. Kukushkin, *Pis'ma JETF* **43**, 79 (1986).

4. D. Weiss, E. Stahl, G. Weiman, K. Ploog, and K. von Klitziug, *Surf. Sci.* **170**, 285 (1986).

5. H.P. Wei, A.M. Chang, D.C. Tsui, and M. Rozeghi, *Phys. Rev. B* **32**, 7016 (1985).

6. Yu.G. Arapov, G.I. Harus, V.N. Neverov, N.G. Shelushinina, M.V. Yakunin, G.A. Alshanskii, and O.A. Kuznetsov, *Nanotechnology* **11**, 351 (2000).

7. Yu.G. Arapov, G.I. Harus, V.N. Neverov, N.G. Shelushinina, M.V. Yakunin, and O.A. Kuznetsov, *JETP* **96**, 118 (2003).

8. D.A. Kozlov, Z.D. Kvon, N.N. Mikhailov, S.A. Dvoretskii, S. Weishäupl, Y. Krupko, and J.-C. Portal, *Appl. Phys. Lett.* **105**, 132102 (2014).

9. T. Khouri, M. Bendias, P. Leubner, C. Brüne, H. Buhmann, L.W. Molenkamp, U. Zeitler, N.E. Hussey, and S. Wiedmann, *Phys. Rev. B* **93**, 125308 (2016).

10. Y.G. Arapov, S.V. Gudina, V.N. Neverov, S.M. Podgornykh, M.R. Popov, G.I. Harus, N.G. Shelushinina, M.V. Yakunin, N.N. Mikhailov, and S.A. Dvoretsky, *Semiconductors* **49**, 1593 (2015).

11. Yu.G. Arapov, S.V. Gudina, V.N. Neverov, S.M. Podgornykh, M.R. Popov, G.I. Harus, N.G. Shelushinina, M.V. Yakunin, S.A. Dvoretsky, and N.N. Mikhailov, *J. Low Temp. Phys.* **185**, 665(2016).

12. M. Konig, H. Buhmann, L. Molenkamp, and T. Hughes, *J. Phys. Soc. Jpn.* **77**, 031007 (2008).

13. M.I.D'yakonov and A.V. Khaetskii, *JETP* **55**, 917 (1982).

14. L.G. Gerchikov and A. Subashiev, *Phys. Status Solidi B* **160**, 443 (1990).

15. E.B. Olshanetsky, S. Sassine, Z.D. Kvon, N.N. Mikhailov, S.A. Dvoretsky, J.C. Portal, and A.L. Aseev, *Pis'ma v JETF* **84**, 661 (2006); Z.D. Kvon, E.B. Olshanetsky, N.N. Mikhailov, and D.A. Kozlov, *Fiz. Nizk. Temp*. **35**, 10 (2009) [*Low Temp. Phys*. **35**, 6 (2009)].

16. M.V. Yakunin, S.M. Podgornykh, N.N. Mikhailov, and S.A. Dvoretsky, *Physica E* **42**, 948 (2010).

17. Yu.G. Arapov, N.A. Gorodilov, V.N. Neverov, M.V. Yakunin, A.V. Germanenko, G.M. Min'kov, O.A. Kuznetsov, R.A. Rubtsova, A.L. Chernov, and L.K. Orlov, *JETP Lett*. **59**, 268 (1994).

18. Y. Guldner, C. Rigaux, M. Grynberg, and A. Mycielski, *Phys. Rev. B* **8**, 3875 (1973).

19. F. Ancilotto, A. Fasolino, and J.C. Maan, *Phys. Rev. B* **38**, 1788(1988).

20. M. Schultz, U. Merkt, A. Sonntag, U. Rössler, R. Winkler, T. Colin, P. Helgesen, T. Skauli, and S. Løvold, *Phys. Rev. B* **57**, 14772 (1998).

21. J.C. Hensel and K. Suzuki, *Phys. Rev. B* **9**, 4219 (1974).

22. R.W. Martin, R.J. Nicholas, G.J. Rees, S.K. Heywood, N.J. Mason, and P.J. Walker, *Phys. Rev. B* **42**, 9237 (1990); R.J. Warburton, R.W. Martin, R.J. Nicholas, L.K. Howard, and M.T. Emeny, *Semicond. Sci. Technol*. **6**, 359 (1991).

23. N.A. Gorodilov, O.A. Kuznetsov, L.K. Orlov, R.A. Rubtsova, A.L. Chernov, N.G. Shelushinina, and G.L. Shtrapenin, *JETP Lett.* **56**, 394 (1992).

24. M.A. Semina and R.A. Suris, *Semiconductors* **49**, 797 (2015).

25. T. Wimbauer, K. Oettinger, A.L. Efros, B.K. Meyer, and H. Brugger, *Phys. Rev. B* **50**, 8889 (1994).

26. A. Pfeuffer-Jeschke, F. Goschenhofer, S.J. Cheng, V. Latussek, J. Gerschütz, C.R. Becker, R.R. Gerhardts, and G. Landwehr, *Physica B* **256–258**, 486 (1998).

27. X.C. Zhang, A. Pfeuffer-Jeschke, K. Ortner, V. Hock, H. Buhmann, C.R. Becker, and G. Landwehr, *Phys. Rev. B* **63**, 245305 (2001).

28. Z.-D. Kvon, S.N. Danilov, N.N. Mikhailov, S. Dvoretsky, W. Prettl, and S. Ganichev, *cond-mat/0708.2175*.

29. P. Svoboda, G. Nachtwei, C. Breitlow, S. Heide, and M. Cukr, *cond-mat/9612053*.

30. B.I. Shklovskii and A.L. Efros, *JETP Lett.* **44**, 669 (1986).

31. A.L. Efros, *Solid State Commun.* **70**, 253 (1989).

32. A.L. Efros, F.G. Pikus, and V.G. Burnett, *Phys. Rev. B* **47**, 2233 (1993).

33. V. Kukushkin, S.V. Meshkov, and V.B. Timofeev, *Phys. Usp.* **31**, 511 (1988).

34. K.S. Novoselov, A.K. Geim, S.V. Morozov, D. Jiang, M.I. Katsnelson, I.V. Grigorieva, S.V. Dubonos, and A.A. Firsov, *Nature* **438**, 197 (2005).